Computational Materials Science 172 (2020) 109325

Contents lists available at ScienceDirect

Computational Materials Science

journal homepage: www.elsevier.com/locate/commatsci

Twinning, phase transformation and dislocation evolution in single crystal titanium under uniaxial strain conditions: A molecular dynamics study

Sunil Rawat*, Nilanjan Mitra

Indian Institute of Technology Kharagpur, Kharagpur 721302, India

ARTICLE INFO

Keywords:
Deformation twinning
HCP metals
Titanium
Molecular dynamics
Phase transformation

ABSTRACT

We perform molecular dynamics simulations to investigate the microstructural evolution and role of twinning on ω-phase transformation in single crystal Ti for loading perpendicular to the c-axis under uniaxial strain conditions. We find that both tension twinning and ω-phase evolve simultaneously and compete with each other. The number of activated tension twin variants not only affects the overall twin volume fraction but also the ω-phase volume fraction. For the case where four twin variants activate, the overall twin volume fraction is lowest and ω-phase volume fraction is highest in comparison to the case where only two twin variants activate. Significant amount of unconsumed parent HCP structure occurs for the case where four twin variants activate in comparison to the case where only two twin variants activate. This suggests that the number of activated twin variants and the spatial distribution of twins belonging to these variants play an important role on the amount of unconsumed parent HCP structure. The presence of high dislocation density for the case where four twin variants activate in comparison to the case where only two variants activate indicates that the number of activated twin variants also affects the overall dislocation density. The foregoing observations can be useful to develop a dynamic material strength model which can account for the coupled evolution of plasticity and phase transformation.

1. Introduction

The HCP metals such as Ti and Zr at ambient temperature and high pressure conditions can transform to a simple hexagonal structure known as ω phase with 3 atoms per unit cell [1–3]. This solid-solid phase transformation can occur under static [2,4] as well as shock loading conditions [3,5] and plays an important role on mechanical properties such as ductility and toughness [1,6]. The experiments on polycrystalline Ti and Zr samples [3,5,7] reported the presence of profuse twinning (reorientations) along with pressure-induced ω phase in shock-recovered samples. Note that the deformation twinning plays an important role on texture evolution [8]. The experiments also reported that the amount of ω phase increased with increase in reorientations (twinning) [3] [Supplemental material [9]]. This means that the microstructure of the material will be governed by the evolution of deformation twinning, dislocations and phase transformation. While it is known that the microstructure of the materials affects the mechanical properties, a fundamental understanding of the microstructural evolution (evolution of dislocations, deformation twinning and phase transformation) of the material under different loading situations is required.

The primary focus of experimental as well as computational studies on Ti and Zr in the literature was to understand the transition pressure for the ω phase [1,2,5], orientation relationship between α and ω phases [6,9–13], role of oxygen content on the phase transformation [5], role of peak pressure on the volume fraction of ω phase [3] and kinetics of reverse ω to α transformation [14,15]. The experiments on polycrystalline Ti [3] showed reorientations (profuse twinning) along with phase transformation and these reorientations increased with increase in volume fraction of ω phase. However, the nature as well as role of deformation twinning on the phase transformation in the experiments is not clear. This is primarily because the experiments were performed on polycrystalline specimens and the deformation modes were obtained from the texture analysis [16].

The classical molecular dynamics (MD) simulations are commonly used to understand the basic mechanisms of deformation and fracture. They are also frequently used to understand the defect evolution dynamics [17–20]. While it is difficult to understand the microstructural evolution in experiments, especially under high strain rate situations, the MD simulations can serve as a useful tool to explore the microstructural evolution of the material under different loading situations. Zong et al. [9,16] performed molecular dynamics (MD) simulations to understand the transformation pathways and orientation relationship between α and ω phases in single crystal Ti with shock loading in different directions. They reported that for c-axis shock compression, α to

* Corresponding author.
E-mail addresses: alig.sunil@gmail.com (S. Rawat), nilanjan@civil.iitkgp.ernet.in (N. Mitra).

https://doi.org/10.1016/j.commatsci.2019.109325
Received 4 June 2019; Received in revised form 27 September 2019; Accepted 29 September 2019
Available online 15 October 2019
0927-0256/

ω phase transformation occurred without any compression twinning while for shock loading perpendicular to the c-axis, they observed 90° rotations along with α to ω phase transformation. However, those simulations mainly focused on the transformation pathways and did not report the evolution dynamics of twinning and phase transformation. Recently, Rawat et al. [13,21] in their MD simulations on single crystal Ti under c-axis uniaxial compressive strain conditions showed that the $\{10\bar{1}1\}$ compression twins activated and assisted the α to ω phase transformation. They also reported the evolution dynamics of extension twinning for loading perpendicular to the c-axis [18]. However, that work [18] was limited to twin evolution dynamics and did not probe the role of twinning on the α to ω phase transformation for loading perpendicular to the c-axis.

In this work, we perform compression perpendicular to the c-axis under uniaxial strain conditions at room temperature using two well-known interatomic potentials [22,23] to investigate the microstructural evolution of the material and understand the role of twinning on the evolution of ω phase in single crystal titanium under uniaxial strain condition.

The constitutive equations to describe the evolution of dislocation slip and deformation twinning in HCP metals have been well described by various researchers [24–27]. However, there is no existing dynamic strength model which can account for the processes such as solid-solid phase transformation for predictive continuum simulations. Moreover, the ω phase transformation is typically described by static or equilibrium phase diagrams which do not depict the time evolution of ω-phase volume fraction. To develop a physics-based dynamic strength model which can account for the coupled evolution of plasticity (dislocation slip and deformation twinning) and phase transformation and to develop a phase diagram under dynamic loading conditions, the microstructural evolution of the material due to plasticity (dislocation slip and twinning) and phase transformation should be understood. In this regard, from a continuum perspective, one would be interested to know: (*a*) What is the role of twinning on the ω-phase evolution? Does it suppress or promote the ω-phase? (*b*) Does the number of activated twin variants affect the volume fraction of ω-phase? (*c*) Does twinning consume the parent HCP structure? (*d*) How dislocation density evolve during the evolution of twinning and ω-phase? (*e*) Does number of activated twin variants affect the overall dislocation density? These and allied questions can provide a way to connect the atomistic information to develop the material strength models which can account for the coupled evolution of plasticity and phase transformation under dynamic loading conditions.

2. Computational method

We use LAMMPS [28] code to simulate the deformation of perfect single crystal titanium under uniaxial strain conditions. These loading conditions are connected to the high velocity impact experiments where the passage of the shock deforms the target material under uniaxial strain conditions [29]. The number of atoms in the simulation domain is 4.6×10^5 atoms and the side length of the simulation domain is 20 nm in each direction. In this set up, the global X-, Y- and Z-directions of the simulation domain are $\langle2\bar{1}\bar{1}0\rangle$, $\langle01\bar{1}0\rangle$ and $\langle0001\rangle$, respectively. We apply periodic boundary conditions in each direction. To integrate the equations of motion, we use velocity-Verlet algorithm. A timestep of 2 femto-second is used to integrate the equations of motion. We use Nose-Hoover thermostat and barostat to control the temperature and pressure of the system. First we equilibrate the system at 300 K temperature and 0 bar pressure using an NPT ensemble up to 40 ps. After equilibration at 300 K and 0 bar pressure, an engineering strain rate of 10^9 s^{-1} is applied to deform the system at a constant temperature of 300 K using an NVT ensemble. We use crystal analysis tool [30] and basal plane vector (BPV) [31] analysis to process the atomistic data. To visualize the obtained results, we use Ovito [32].

We perform compression along $\langle2\bar{1}\bar{1}0\rangle$ and $\langle01\bar{1}0\rangle$ directions and categorize the loading conditions as *case A* for compressive loading along $\langle2\bar{1}\bar{1}0\rangle$ direction and *case B* for compressive loading along $\langle01\bar{1}0\rangle$ direction (Fig. 1). For *case A* where compressive loading is applied along X-direction ($\langle2\bar{1}\bar{1}0\rangle$ direction), the Y- and Z-directions are constrained so that the side lengths of the simulation domain along these directions should not change during the deformation. Similarly, for *case B* where compressive loading is applied along Y-direction ($\langle01\bar{1}0\rangle$ direction), the X- and Z-directions are constrained so that the side lengths of the simulation domain along these directions remain constant during the deformation.

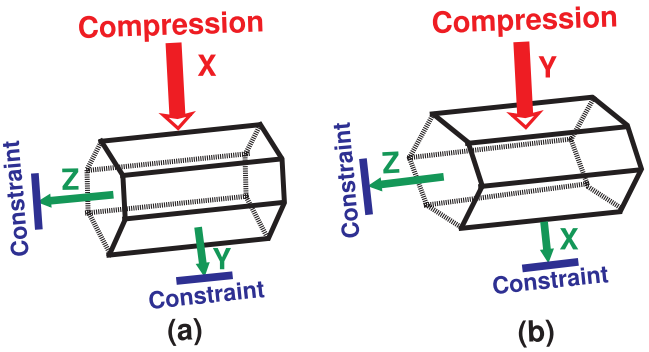

Fig. 1. Applied loading conditions. Here open arrows (red) refer to the loading directions ($\langle2\bar{1}\bar{1}0\rangle$ (case A) and $\langle01\bar{1}0\rangle$ (case B)) while solid arrows (green) refer to the constrained directions. The size of the constrained direction does not change during the deformation.

3. Results and discussion

For Ti, it is well known that the applied strain can result in twinning as well as α to ω phase transformation [3,5,7,9,13,21]. In this regard, first we investigate the structural evolution of the material under the applied loading conditions by performing CAT analysis [30]. This analysis provides information on the overall HCP structure (atoms belonging to parent as well as twins), stacking faults and unknown structure (atoms which do not correspond to any known crystal structures, e.g. FCC, HCP, BCC etc.). Note that the twinned atoms belong to an HCP structure while atoms belonging to an ω phase correspond to an unknown structure [13,21].

Fig. 2 shows the evolution of overall HCP structure (number fraction corresponding to parent as well as twins), unknown structure and stacking faults obtained with the Kim and the Hennig potentials for each case of the loading conditions. As observed from Fig. 2 that the Hennig potential shows large number fraction corresponding to overall HCP structure in comparison to the Kim potential for each case of the loading conditions. In this regard, it should be noted that for both loading conditions where compressive loading is applied perpendicular to the c-axis, the activation of tension twin systems is expected [18]. This means that the large number fraction corresponding to the overall HCP structure with the Hennig potential in each case of the loading conditions could be due to the high growth of the twins in comparison to the Kim potential [18]. From Fig. 2, it is also observed that the Kim potential shows large number fraction corresponding to unknown structure in comparison to the Hennig potential for both loading conditions. Note that the compressive loading under uniaxial strain conditions may also lead to the possible structural α to ω phase transformation [9,13,16]. This means that the large number fraction for unknown structure with the Kim potential could be due to the possible structural phase transformation which can obstruct the growth of twins and consume the parent HCP structure.

Fig. 3 shows the snapshots for HCP and unknown structures obtained with the Kim and the Hennig potentials for case A and case B loading conditions. As observed from Fig. 3 that the orientation of some of the atomic clusters belonging to HCP structure is different from the

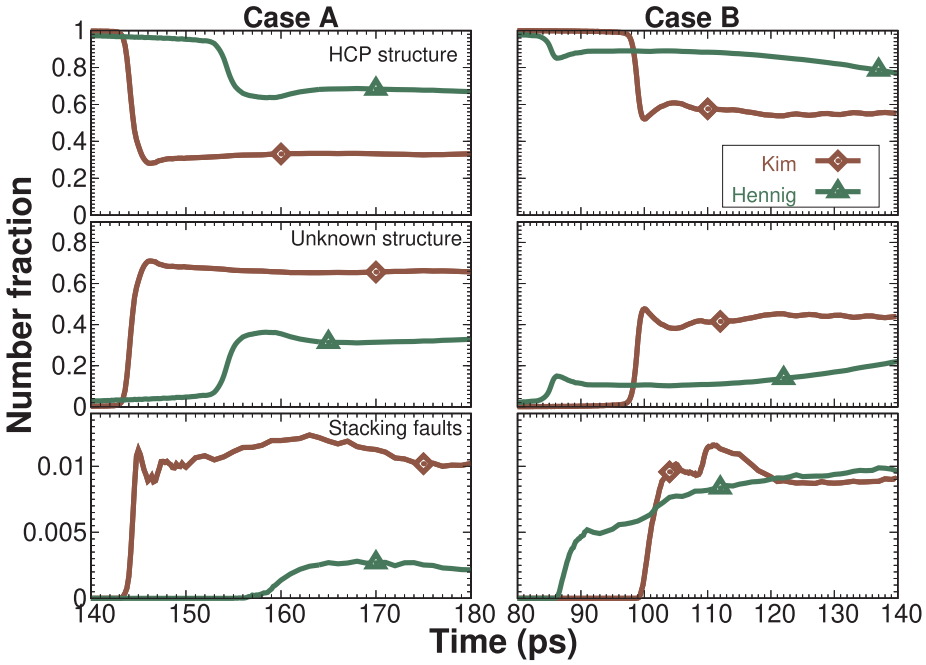

Fig. 2. Time evolution of number fraction belonging to overall HCP structure (parent as well as twins), stacking faults and unknown structure (atoms which do not belong to any known crystal structures, such as FCC, BCC etc.) for each case of the loading conditions with the Kim and the Hennig potentials.

parent HCP structure indicating the rotation of the c-axis (twinning). This means that the HCP structure includes both parent as well as twinned volumes. It is also observed from Fig. 3 that for each case of the loading conditions with both potentials, the unknown structure is oriented similar to twinned volumes which could be due to the ω-phase transformation. In this regard, note that the shock experiments on polycrystalline samples [3,5,7] reported the twinning along with phase transformation. In addition to this, the MD simulations on single crystal Ti [9,16] under shock loading conditions also reported the 90° rotations along with the phase transformation. However, the simulations [9,16] did not show the evolution of microstructures which we present in this paper albeit with loading conditions different from [9,16].

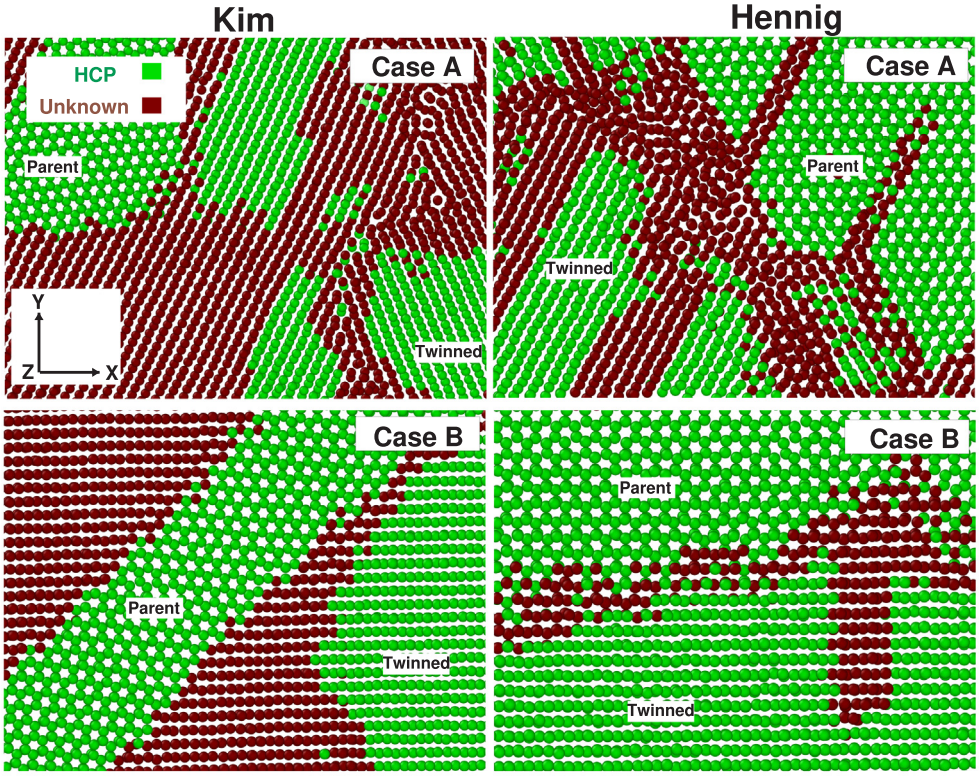

Fig. 3. Snapshots for HCP and unknown structures obtained with the Kim and the Hennig potentials for case A (170 ps) and case B (110 ps) loading conditions. Here HCP structure includes both parent HCP structure and twinned volumes [18].

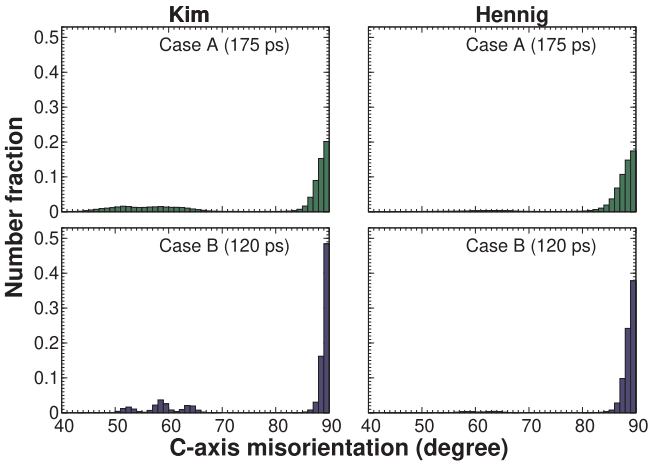

Fig. 4. C-axis misorientation distribution obtained with the Kim and the Hennig potentials for both loading conditions.

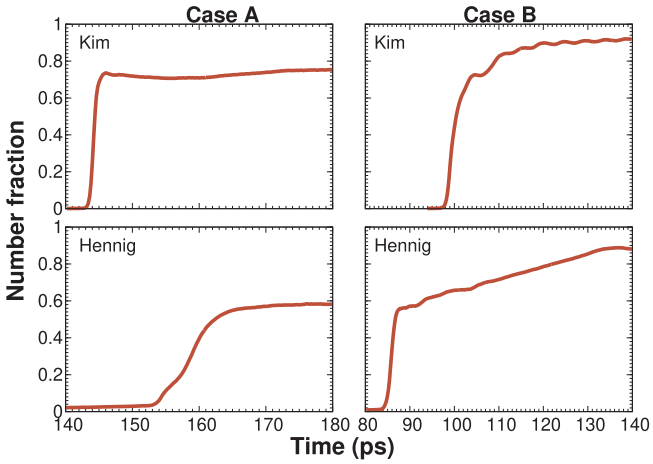

Fig. 5. Overall reorientations (number fraction corresponding to 50–70° and 85–90° peaks in Fig. 4) as a function of time for both loading conditions with the Kim and the Hennig potentials.

3.1. C-axis misorientations and overall reorientations

To understand the c-axis misorientations due to deformation (Fig. 3), we perform c-axis misorientation analysis. The c-axis misorientation is defined as the angle between the initial (at t = 0) and instantaneous c-vectors for each atom in the simulation domain. In this analysis, we exclude those highly disordered atoms for which c-vector is not computed. Fig. 4 shows the c-axis misorientation distribution obtained with the Kim and the Hennig potentials for both loading conditions. As observed from Fig. 4, the misorientation peaks occur in the range of 50–70° and 85–90° indicating reorientation of the parent matrix (rotation of the c-axis). The 50–70° peaks in the misorientation distribution (Fig. 4) indicate the possible α to ω phase transformation [13,21] while 85–90° peaks indicate the activation of tension twins [18]. Note that the misorientation peak corresponding to 90° in Fig. 4 dominates over the other peaks for each case of the loading condition with both potentials indicating dominance of the 90° rotations. These 90° rotations have been observed in MD simulations [9,16] as well as in experiments [33]. Qualitatively, both potentials show 50–70° and 85–90° peaks in the misorientation angle distribution. However, the magnitude of the peaks with the Kim potential is larger compared to that with the Hennig potential in each case of the loading conditions.

To understand quantitatively the amount of 50–70° and 85–90° peaks in the misorientation angle distribution (Fig. 4), we compute the number fraction corresponding to these peaks. Fig. 5 shows the overall reorientations (number fraction corresponding to 50–70° and 85–90° peaks in Fig. 4) as a function of time for both loading conditions with the Kim and the Hennig potentials.

As observed from Fig. 5 that for each case of the loading conditions, the overall reorientations (number fraction corresponding to 50–70° and 85–90° peaks in Fig. 4) with the Kim potential dominates over that with the Hennig potential. Note that the shock experiments on Ti and Zr [3,5] [Supplemental material [16]] observed the reorientations (twinning) along with ω phase transformation and found a correlation between the overall reorientations and ω-phase volume fraction. In those experiments [3,5,16], the high volume fraction of ω-phase was correlated with the high reorientations. This means that the high reorientations with the Kim potential could be due to an overall dominance of twinning and ω phase in comparison to that with the Hennig potential. Note also that the overall reorientations for case B dominates over that for case A with each case of the potentials used. This could be due to the activation of few twin variants for case B in comparison to case A where activation of more number of twin variants may suppress the growth of twins and thereby lead to smaller twinned volumes [17,18]. Apart from that the structural phase transformation can also suppress the growth of the twins [13].

3.2. Overall twin volume fraction

Recently, Rawat et al. [18] in their MD simulations on single crystal Ti found that the activated twinning did not consume the entire parent HCP structure. They also reported that the saturation of overall twin volume fraction could be due to the unavailability of parent HCP structure, suppression of twin growth due to twins of other variants and presence of some other deformation mechanism such as phase transformation. However, that work [18] did not probe whether the twinning consumed the entire available parent HCP structure or not. Here we present twin analysis to understand (*i*) whether the twinning consumes the entire available parent HCP structure (*ii*) the contribution of overall twinning to the overall reorientations and (*iii*) role of activated twin variants on the overall reorientations (50–70° and 85–90° peaks in Fig. 4).

Since the compressive loading is applied perpendicular to the c-axis, the tension twins (also known as extension twins) should activate for each case of the loading conditions [17,18]. The commonly reported tension twins in Ti at room temperature are $\{10\bar{1}2\}$ and $\{11\bar{2}1\}$ [34]. The Schmid factor for $\{10\bar{1}2\}$ twins is 0.37 for case A and 0.5 for case B. While Schmid factor for $\{11\bar{2}1\}$ twins is 0.28 for case A and 0.21 for case B. We found that only $\{10\bar{1}2\}$ twins activate for both loading conditions [18]. Note that there are six possible variants of $\{10\bar{1}2\}$ $\langle\bar{1}011\rangle$ twin system and the activation of these twin variants depends on the applied loading conditions. For case A, four variants of $\{10\bar{1}2\}$ $\langle\bar{1}011\rangle$ twin system activate while two variants of $\{10\bar{1}2\}$ $\langle\bar{1}011\rangle$ twin system activate for case B [18]. For the sake of completeness, here we briefly describe the twin variant volume fraction and overall twin volume fraction for both loading conditions with the Kim and the Hennig potentials. A detailed discussion on the twin evolution dynamics for both loading conditions with the Kim and the Hennig potentials is described elsewhere [18] and will not be presented in this manuscript.

The ab initio simulations and theoretical calculations showed that the thickness of a stable twin should be $\geqslant$6 layers [35–37] which correspond to around 100 atoms [17]. Therefore, to compute the twin volume fraction, we consider only those twins which contain atoms $\geqslant$100. Fig. 6 shows the time evolution of number fraction corresponding to overall twinned volume for both loading conditions with the Kim and the Hennig potentials [18]. The number fraction corresponding to each activated twin variant is also shown in Fig. 6. To understand whether the activated twinning consumes the entire available parent HCP structure, the number fraction corresponding to overall HCP structure is also shown in Fig. 6.

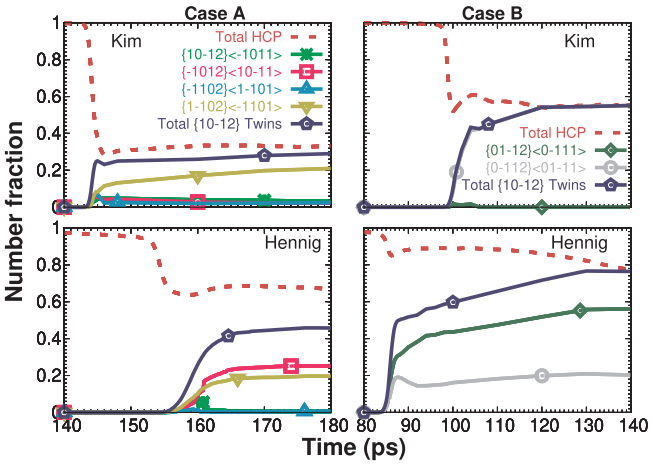

Fig. 6. Time evolution of number fraction corresponding to overall HCP structure and overall twinned volumes for both loading conditions with the Kim and the Hennig potentials. The number fraction corresponding to each activated twin variant is also shown.

As observed from Fig. 6 that for case A, four twin variants activate while for case B, only two twin variants activate both with the Kim and the Hennig potentials [18]. The overall twin volume fraction for each case of the loading conditions with the Hennig potential dominates and contributes most to the overall reorientations (50–70° and 85–90° peaks in Fig. 4) in comparison to the Kim potential. This is due to the rapid growth of twins for case A with the Hennig potential in comparison to the Kim potential [18]. For case A where four twin variants activate, the contribution of overall twinning to the overall reorientations is small while it is large for case B where only two twin variants activate. Note that for each case of the loading conditions with the Kim potential, only one twin variant has significant contribution to the overall twin volume fraction while there are two twin variants which have significant contribution to the overall twin volume fraction for each case of the loading conditions with the Hennig potential. This indicates that the spatial distribution of the twins for the Kim potential is different from that for the Hennig potential. Note also that the $\{10\bar{1}2\}$ twins in case A with both potentials (Fig. 6) do not consume the entire available parent HCP structure (as number fraction corresponding to the overall twinned volume is smaller than that corresponding to the overall HCP structure), while they consume in case B with the Kim potential (number fraction corresponding to the overall twinned volume is equal to that corresponding to the overall HCP structure). For case B with the Hennig potential, there is still a very small number fraction corresponding to the parent HCP structure which is not consumed by twinning (Fig. 6). This is reasonable since the activation of four variants (two conjugate pairs) in case A hinders the growth of the twins of other variants. While in case B where only two variants (one conjugate pair) activate, there is no obstacle in the growth of twins due to other conjugate variants and thereby they can consume the entire available parent HCP structure (e.g. case B with the Kim potential). However, the spatial distribution of twins may also affect the amount of parent HCP structure consumed by twinning even for the case where only two twin variants (one conjugate pair) activate (e.g. case B with the Hennig potential).

3.3. ω phase volume fraction

In previous section (Section 3.2), we have seen that four twin variants (two conjugate pairs) activate for case A while only two variants (one conjugate pair) activate for case B [18]. Note that for case A where four variants (two conjugate pairs) activate (c.f. Fig. 6), the 50–70° peaks in the misorientation distribution (Fig. 4) can occur due to the misorientations between the conjugate variants which is 60° [38]. However, for case B where only two variants (one conjugate pair) activate, the 50–70° peaks can not occur due to the misorientations between the variants since the misorientation between the variants of a conjugate pair is < 10° [38]. Moreover, the $\{10\bar{1}1\}$ twins (compression twins) (for which the theoretical misorientation angle is 57.2° [34]) can not activate for loading perpendicular to the c-axis. This means that the 50–70° peaks in the misorientation angle distribution are neither due to compression twins nor due to the misorientations between the variants. In this regard, it should be noted that the shock experiments on Ti and Zr [3,5] [Supplemental material [16]] observed the reorientations (twinning) along with ω phase transformation. It should also be noted that in our previous work on c-axis compression of single crystal Ti under uniaxial strain conditions with the Kim and the Hennig potentials [13,21], the structure factor analysis showed that the 50–70° and 85–90° peaks in the misorientation distribution was due to the ω phase transformation. In addition to this, one of the possible pathways for α to ω phase transformations was $\{0001\}_\alpha||\{10\bar{1}1\}_\omega$; $\langle 10\bar{1}0\rangle_\alpha||\langle\bar{1}011\rangle_\omega$ [6,11–13,21]. This means that the 50–70° and 85–90° peaks in the misorientation angle distribution (Fig. 4) are possibly due to the ω phase transformation.

To confirm whether the 50–70° and 85–90° peaks in the misorientation angle distribution (Fig. 4) belong to an ω phase, we compute the per-atom structure factor ($S(\mathbf{k}) = \sum_n e^{i\mathbf{k}.\mathbf{r}_n}$) [39] corresponding to different (hkl) planes for α [40] and ω [2,41] phases. To compute per atoms structure factor, we consider only those atoms which belong to unknown structure and show 50–70° and 85–90° peaks in the misorientation distribution (Fig. 4). Fig. 7 shows the structure factor for twin-like oriented unknown structure (atoms with 50–70° and 85–90° peaks in the misorientation angle distribution) for both loading conditions with the Kim and the Hennig potentials. As observed from Fig. 7, the peaks corresponding to ω phase occur for both loading conditions with the Kim and the Hennig potentials. This confirms that the twin-like oriented unknown structure which shows 50–70° and 85–90° peaks in the misorientation angle distribution (Fig. 4) is due to the pressure-induced ω phase transformation. To quantify the amount of ω phase generated for both loading conditions with the Kim and the Hennig potentials and to understand its contribution to the overall reorientations (Fig. 5), we perform c-vector analysis for the twin-like oriented unknown structure (atoms which do not belong to any known crystal structure and show 50–70° and 85–90° peaks in the misorientation angle distribution). For c-vector analysis of the twin-like oriented unknown structure (Fig. 2), we use c-vectors belonging to $\{10\bar{1}2\}$ and $\{10\bar{1}1\}$ twins to confirm whether the atoms belonging to 50–70° and 85–90° peaks in the misorientation distribution (Fig. 4) have twin-like orientations. Fig. 8 shows the time evolution of ω-phase volume fraction as well as the number fraction corresponding to overall reorientations (50–70° and 85–90° peaks in Fig. 5) for both loading conditions with the Kim and the Hennig Potentials.

As observed from Fig. 8 that the ω-phase volume fraction for each case of the loading conditions with the Kim potentials contribute significantly to the overall reorientations (number fraction corresponding to 50–70° and 85–90° peaks in Fig. 5). While its contribution to the overall reorientations with the Hennig potential for each case of the loading conditions is quite small. Apart from that the ω-phase volume fraction for each case of the loading conditions with the Kim potentials dominates over that with the Hennig potential. In previous section (Section 3.2), we have seen that the overall twin volume fraction for each case of the loading conditions with the Hennig potentials was larger than that with the Kim potential (c.f. Fig. 6). This means that the Hennig potential shows twinning dominated deformation in each case of the loading conditions while the Kim potential shows a competitive response of twinning and ω-phase to accommodate the applied strain for each case of the loading conditions. Note that for case A with the Kim potential where four tension twin variants (two conjugate pairs) activate (c.f. Fig. 6), the volume fraction of ω phase is large compared to the case B where only two tension twin variants (one conjugate pair) activate. This indicates that the number of activated twin variants

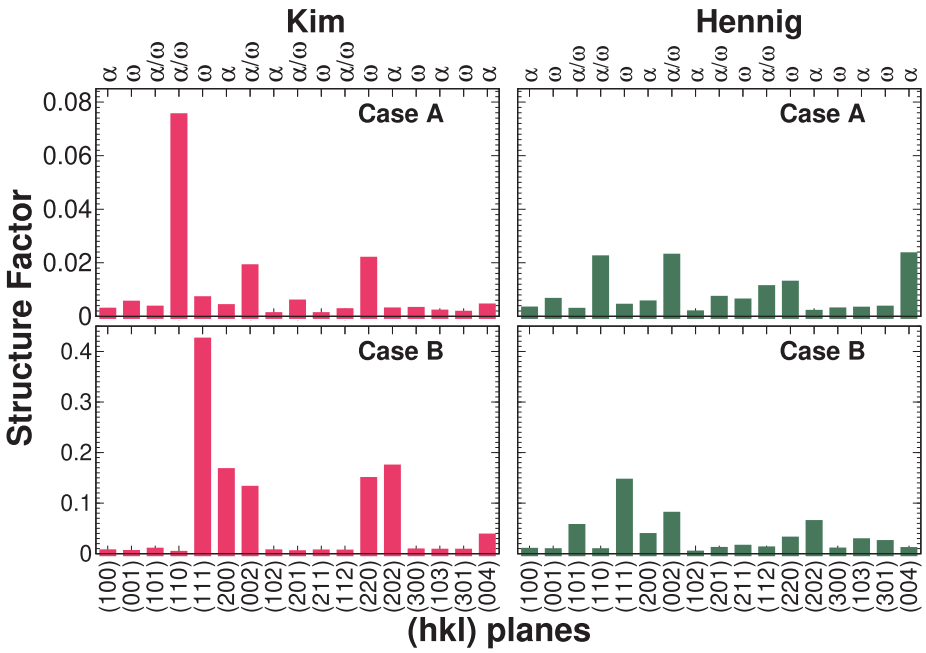

Fig. 7. Per-atom structure factor for twin-like oriented unknown structure (atoms corresponding to 50–70° and 85–90° peaks in the misorientation angle distribution) for *case A* (180 ps) and *case B* (140 ps) loading conditions with the Kim and the Hennig potentials.

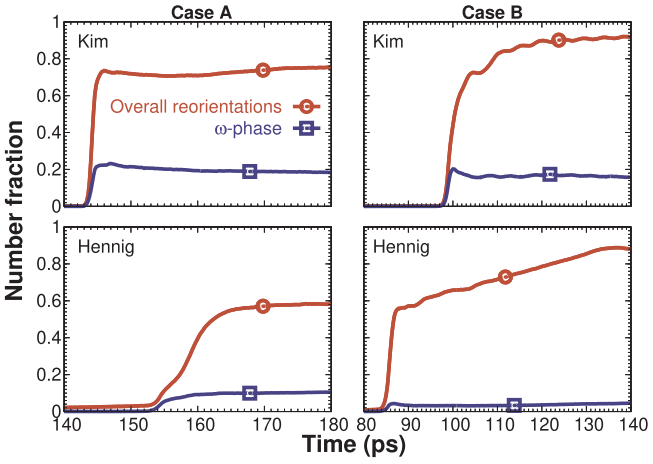

Fig. 8. The volume fraction of ω-phase as a function of time for both loading conditions with the Kim and the Hennig potentials. The overall reorientations (number fraction corresponding to 50–70° and 85–90° peaks in Fig. 5) for each case of the loading conditions are also shown for comparison.

affects not only the overall twin volume fraction (c.f. Fig. 6) but also the volume fraction of ω phase. More number of activated twin variants with the Kim potential leads to a smaller overall twin volume fraction (c.f. Fig. 6) and larger volume fraction of ω phase. A similar trend is also observed with the Hennig potential for both loading conditions. However, the volume fraction of ω-phase with the Hennig potential is relatively quite small in comparison to the Kim potential for each case of the loading conditions.

Fig. 9 shows the parent HCP structure, $\{10\bar{1}2\}$ twins, ω-phase and unknown structure for case A loading condition with the Kim potential.

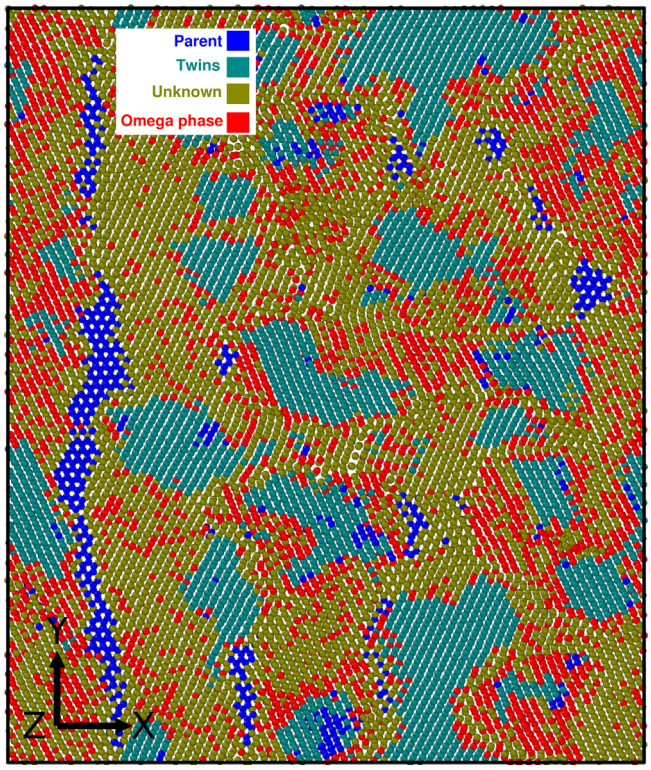

Fig. 9. Snapshot showing parent HCP structure, $\{10\bar{1}2\}$ twins, ω-phase and unknown structure for case A (146 ps) loading condition with the Kim potential.

3.4. Dislocation density

To understand the evolution of dislocation density during the evolution of twinning and ω-phase for each case of the loading conditions with the Kim and the Hennig potentials, we perform dislocation analysis using Dislocation Extraction Algorithm (DXA) implemented in Ovito [32]. For Ti, the most common slip systems which can activate under the given loading conditions are prismatic ⟨a⟩ and pyramidal ⟨c + a⟩ slip systems [42–44]. However, the pyramidal ⟨c + a⟩ slip system does not activate at room temperature due to a very high critical resolved shear stress (CRSS) in comparison to the prismatic ⟨a⟩ slip system [45,46].

From the Burgers vector analysis, we identify $1/3\langle 1\bar{2}10\rangle$ prismatic dislocations, $1/3\langle 1\bar{1}00\rangle$ partial dislocations on basal slip systems and

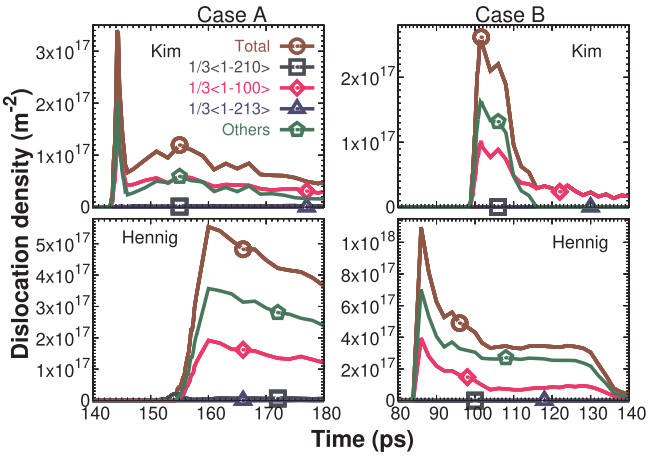

Fig. 10. Evolution of dislocation density as a function of time for both loading conditions with the Kim and the Hennig potentials.

$1/3\langle 1\bar{2}13\rangle$ pyramidal dislocations. In addition to these dislocations, there are some dislocations which are unidentifiable. We call them "other dislocations". Fig. 10 shows the time evolution of dislocation density for each case of the loading conditions with the Kim and the Henning potentials.

As observed from Fig. 10 that for each case of the loading conditions with the Kim and the Hennig potentials, the dislocation density increases, reaches a peak and then decreases during the evolution of twinning and ω-phase transformation. The overall dislocation density with the Hennig potential is large compared to that with the Kim potential for each case of the loading conditions. In this regard, it should be noted that the stacking fault energy (213 mJ m^{-1}) for the Kim potential is higher than that for the Hennig potential (170 mJm^{-1}) while experimentally reported stacking fault energy for titanium is 300 mJ m^{-1} [47]. It is known that the large dislocation dissociation into partials and high dislocation density occur for the low value of stacking fault energy [48]. This means that the Hennig potential with the low stacking fault energy will have high dislocation density in comparison to the Kim potential which has comparatively high stacking fault energy. This is what we observed in Fig. 10. This means that the dislocation density strongly correlates with the stacking fault energy. Note that the Hennig potential shows the large overall twin volume fraction and small volume fraction of ω-phase in comparison to the Kim potential. This indicates that the applied deformation for the Hennig potential is primarily accommodated by twinning and dislocation slip. While for the Kim potential where the overall dislocation density is small in comparison to the Hennig potential, the applied deformation is primarily accommodated by twinning and ω-phase transformation.

It is also observed from Fig. 10 that only partial dislocations on the basal slip system and other dislocations make significant contribution to the overall dislocation density for each case of the loading conditions with the Kim and the Hennig potentials. For the Hennig potential, the other dislocations dominate over the $1/3\ \langle 1\bar{1}00\rangle$ dislocations and contribute most to the overall dislocation density for each case of the loading conditions. While for the Kim potential, the other dislocations compete with the $1/3\ \langle 1\bar{1}00\rangle$ dislocations for case A while for case B, the other dislocations dominate and contribute most to the overall dislocation density up to some time point (~110 ps) and then they disappear. After that the $1/3\ \langle 1\bar{1}00\rangle$ dislocations for case B with the Kim potential are the only contributor to the overall dislocations. Note that the other dislocations lie on the twin-matrix interface [17] and for case B with the Kim potential, there is no twin-matrix interface since the entire available parent HCP structure is consumed by twinning (Fig. 6). This is why the other dislocation density for case B with the Kim potential becomes zero. This means that the large number of twin-matrix interfaces leads to a large dislocation density corresponding to other dislocations. This indicates a correlation between the dislocation density corresponding to the other dislocations and the amount of unconsumed parent HCP structure (c.f. Fig. 6). Large density of other dislocations corresponds to the large amount of unconsumed parent HCP structure for each case of the loading conditions with both potentials. For example, for case A with the Kim potential, the amount of unconsumed parent HCP structure is 7.1% at 160 ps while for the same loading condition (case A) with the Hennig potential, there is a 38% parent HCP structure at 160 ps which is not consumed by twinning. This means that there is a large number of twin-matrix interfaces for case A at 160 ps with the Hennig potential in comparison to that with the Kim potential and thereby leads to a large density of other dislocations for case A with the Hennig potential. For case B where twinning consumes the entire parent HCP structure with the Kim potential (c.f. Fig. 6), the "other" dislocations disappear (Fig. 10) while they decrease by an order of magnitude with the Hennig potential.

Table 1
Details of the overall reorientations, overall HCP structure, parent HCP structure, Overall twin volume fraction, ω-phase volume fraction and dislocation density for case A (180 ps) and case B (140 ps) with both potentials.

	Kim		Hennig	
	Case A	Case B	Case A	Case B
Overall reorientations (%)	75.2	91.8	58.0	88.0
Overall HCP structure (%)	33.2	55.1	67.0	77.0
Overall twin volume fraction (%)	29.0	55.1	45.7	76.4
Parent HCP structure (%)	4.2	0	21.3	0.6
ω-phase volume fraction (%)	18.4	15.8	10.4	4.5
$1/3\langle 1\bar{2}10\rangle$ dislocation density (m^{-2})	2.23×10^{15}	0	6.13×10^{15}	0
$1/3\ \langle 1\bar{1}00\rangle$ dislocation density (m^{-2})	2.75×10^{16}	1.70×10^{16}	1.21×10^{17}	1.97×10^{16}
$1/3\langle 1\bar{2}13\rangle$ dislocation density (m^{-2})	0	0	0	0
Other dislocation density (m^{-2})	1.29×10^{16}	0	2.38×10^{17}	2.39×10^{16}
Overall dislocation density (m^{-2})	4.27×10^{16}	1.70×10^{16}	3.65×10^{17}	4.36×10^{16}

Table 1 shows the details of the overall reorientations, overall HCP structure, parent HCP structure, overall twin volume fraction, ω-phase volume fraction and dislocation density for case A (180 ps) and case B (140 ps) with the Kim and the Hennig potentials. As observed from Table 1 that the least dislocation density corresponds to the case B with the Kim potential where there is no availability of the parent HCP structure while highest dislocation density occurs for the case A with the Hennig potential where the highest parent HCP structure is available.

3.5. Statistical analysis

To understand the variations in the overall twin volume fraction, ω-phase volume fraction and overall dislocation density, we perform statistical analysis. We consider 10 samples for each loading condition with the Kim potential. This means that we perform a total of 20 simulations for both loading conditions with the Kim potential. We exclude the Hennig potential for this analysis due to a very high computational time required to perform the analyses (2–3 times higher computational time is required to simulate one sample with the Hennig potential). To introduce the randomness in the simulations, we use a different random number seed for each sample to initialize the atomic velocities using Gaussian distribution at 300 K and equilibrate the sample at 300 K and 0 bar pressure using an NPT ensemble with the Kim potential. After equilibration, we deform the sample at 10^9 s^{-1} engineering strain rate with the Kim potential under case A and case B loading conditions. We compute overall reorientations, overall twin

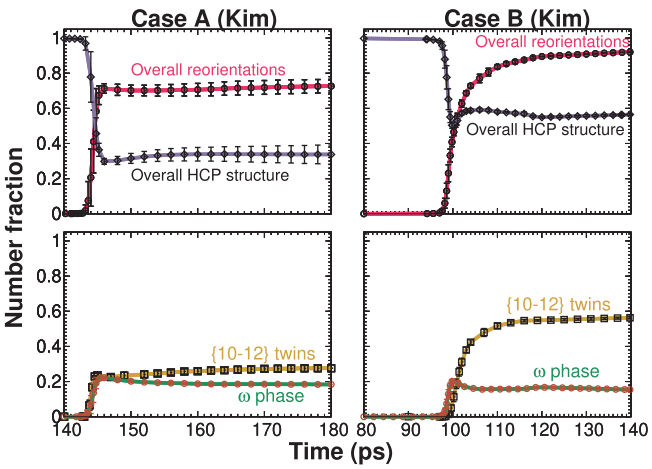

Fig. 11. Overall reorientations (number fraction corresponding to 50–70° and 85–90° peaks in Fig. 4), overall twin volume fraction and ω-phase volume fraction as a function of time for each case of the loading conditions with the Kim potential.

volume fraction, ω-phase volume fraction and overall dislocation density for each sample for both loading conditions.

3.5.1. Overall reorientations, twinning and ω-phase

We perform statistical average of overall reorientations (number fraction corresponding to 50–70° and 85–90° peaks in Fig. 4), overall twin volume fraction and ω-phase volume fraction. Fig. 11 shows the statistically averaged number fraction corresponding to overall reorientations, twinning and ω-phase for both loading conditions with the Kim potential. As observed from Fig. 11 that the variations in the overall reorientations for case A are quite significant, especially in the initial evolution regime. These large variations mostly correspond to the variations in the initial evolution regime of the ω-phase volume fraction. While for case B, the variations in the number fraction corresponding to overall reorientations as well as the ω-phase volume fraction are quite small in comparison to case A. Note that the variations in the overall twin volume fraction for each case of the loading conditions are not significant. Note also that for case A where four twin variants (two conjugate pairs) activate, the overall twin volume fraction competes with the ω-phase volume fraction in the initial evolution regime and then dominates over the ω-phase volume fraction. While for case B, the activation of twins is slightly delayed in comparison to ω-phase but later the overall twin volume fraction dominates over the ω-phase volume fraction. For the case where four twin variants activate (case A), the ω-phase volume fraction is highest and the overall twin volume fraction is lowest in comparison to the case where only two variants activate (case B). This means that the number of activated twin variants not only affects the overall twin volume fraction but also the ω-phase volume fraction.

3.5.2. Overall dislocation density

We perform statistical average of overall dislocation density for both loading conditions with the Kim potential. Fig. 12 shows the statistical average of overall dislocation density as a function of time for each case of the loading conditions with the Kim potential. As observed from Fig. 12 that the variations in overall dislocation density for case A are quite large, especially in the initial evolution regime of the overall dislocation density. These variations are also quite significant for case B. Note that for case A, four twin variants (two conjugate pairs) activate while only two twin variants (one conjugate pair) activate for case B. This means that the large variations in the overall dislocation density for case A are possibly due to the large variations in the twin-matrix interfaces in comparison to case B.

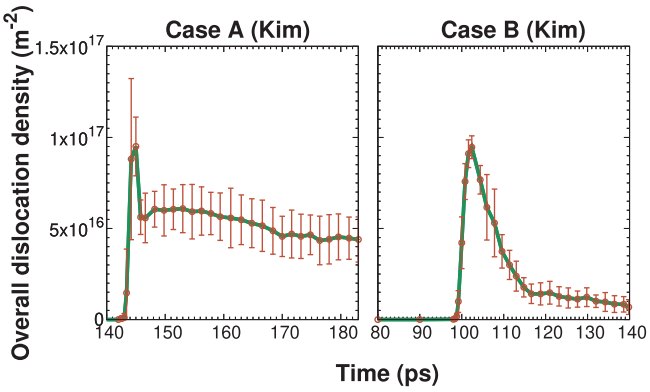

Fig. 12. Statistical average of overall dislocation density as a function of time for both loading conditions with the Kim potential.

4. Summary and conclusions

We perform compression of single crystal Ti along $\langle 2\bar{1}\bar{1}0\rangle$ and $\langle 01\bar{1}0\rangle$ directions at room temperature to investigate the microstructural evolution and role of twinning on ω-phase under uniaxial strain conditions using two well-known interatomic potentials. The compressive strain applied perpendicular to the c-axis results in the activation of $\{10\bar{1}2\}$ twinning as well as the ω-phase transformation. The activation of four $\{10\bar{1}2\}$ variants for loading along $\langle 2\bar{1}\bar{1}0\rangle$ direction leads to a different microstructural evolution from the loading along $\langle 01\bar{1}0\rangle$ direction where only two variants activate. The main conclusions of the present study are as follows:

- Twinning and phase transformation evolve simultaneously and compete with each other.
- The volume fraction of the ω-phase for the case where four twin variants activate is large in comparison to the case where only two twin variants activate. On the other hand, the overall twin volume fraction for the case where four twin variants activate is small in comparison to the case where only two twin variants activate. This means that the number of activated twin variants and their spatial distribution not only affects the overall twin volume fraction but also the volume fraction of the ω-phase. This suggests a correlation among the number of activated twin variants, overall twin volume fraction and ω-phase volume fraction. The large number of activated twin variants leads to a smaller overall twin volume fraction and larger volume fraction of ω-phase.
- For the case where only two twin variants (one conjugate pair) activate, twinning consumes the entire available parent HCP structure for the Kim potential while a very small amount (0.6%) of parent HCP structure remains unconsumed for the Hennig potential. This suggests that the spatial distribution of the twins for the Kim potential is different from that for the Hennig potentials.
- For the case where four twin variants (two conjugate pairs) activate, the amount of unconsumed parent HCP structure is significant for both the Kim (4%) and the Hennig (21%) potentials. This suggests that not only the spatial distribution of the twins but also the number of activated twin variants affects the amount of unconsumed parent HCP structure.
- During the evolution of the twinning and the ω-phase, the dislocation density increases, reaches a peak and then decreases. The overall dislocation density peaks corresponding to the onset of saturation of overall twin volume fraction.
- The overall dislocation density for the case where four twin variants activate is high in comparison to the case where only two twin variants activate. This means that the number of activated twin variants also affects the overall dislocation density.
- High dislocation density, large overall twin volume fraction and

small ω-phase volume fraction for the Hennig potential indicate that the applied deformation is primarily accommodated by the twinning and the dislocation slip.
- Low dislocation density, large overall twin volume fraction and large ω-phase volume fraction for the Kim potential indicate that the applied deformation is primarily accommodated by the twinning and the ω-phase.

These observations should help in constructing the dynamic material strength models which can account for the evolution of plasticity as well as phase transformation. To gain further understanding on the evolution dynamics, it would be interesting to investigate the role of temperature on the evolution dynamics of twinning and phase transformation.

Data availability

The data required to reproduce these findings cannot be shared at this time since the data also forms part of an ongoing study.

CRediT authorship contribution statement

Sunil Rawat: Methodology, Software, Visualization, Investigation, Writing - original draft, Data curation, Formal analysis, Validation, Writing - review & editing. **Nilanjan Mitra:** Supervision, Resources, Writing - original draft, Writing - review & editing.

Declaration of Competing Interest

The authors declare that they have no known competing financial interests or personal relationships that could have appeared to influence the work reported in this paper.

References

[1] S. Sikka, Y. Vohra, R. Chidambaram, Omega phase in materials, Prog. Mater. Sci. 27 (3) (1982) 245–310.
[2] D. Errandonea, Y. Meng, M. Somayazulu, D. Häusermann, Pressure-induced $\alpha\omega$ transition in titanium metal: a systematic study of the effects of uniaxial stress, Physica B 355 (1) (2005) 116–125.
[3] E. Cerreta, J. Escobedo, P. Rigg, C. Trujillo, D. Brown, T. Sisneros, B. Clausen, M. Lopez, T. Lookman, C. Bronkhorst, et al., The influence of phase and substructural evolution during dynamic loading on subsequent mechanical properties of zirconium, Acta Mater. 61 (20) (2013) 7712–7719.
[4] Y. Vohra, S. Sikka, S. Vaidya, R. Chidambaram, Impurity effects and reaction kinetics of the pressure-induced $\alpha\omega$ transformation in ti, J. Phys. Chem. Solids 38 (11) (1977) 1293–1296.
[5] E. Cerreta, G. Gray III, A. Lawson, T. Mason, C. Morris, The influence of oxygen content on the α to ω phase transformation and shock hardening of titanium, J. Appl. Phys. 100 (1) (2006) 013530 .
[6] D. Trinkle, R. Hennig, S. Srinivasan, D. Hatch, M. Jones, H. Stokes, R. Albers, J. Wilkins, New mechanism for the α to ω martensitic transformation in pure titanium, Phys. Rev. Lett. 91 (2) (2003) 025701 .
[7] E. Cerreta, G. Gray, R. Hixson, P. Rigg, D. Brown, The influence of interstitial oxygen and peak pressure on the shock loading behavior of zirconium, Acta Mater. 53 (6) (2005) 1751–1758.
[8] F. Xu, X. Zhang, H. Ni, Y. Cheng, Y. Zhu, Q. Liu, Effect of twinning on microstructure and texture evolutions of pure ti during dynamic plastic deformation, Mater. Sci. Eng.: A 564 (2013) 22–33.
[9] H. Zong, T. Lookman, X. Ding, S.-N. Luo, J. Sun, Anisotropic shock response of titanium: reorientation and transformation mechanisms, Acta Mater. 65 (2014) 10–18.
[10] J. Silcock, An x-ray examination of the to phase in tiv, timo and ticr alloys, Acta Metall. 6 (7) (1958) 481–493.
[11] M. Usikov, V. Zilbershtein, The orientation relationship between the α and ω-phases of titanium and zirconium, Physica Status Solidi (a) 19 (1) (1973) 53–58.
[12] S. Song, G. Gray III, Microscopic and crystallographic aspects of retained omega phase in shock-loaded zirconium and its formation mechanism, Philos. Mag. A 71 (2) (1995) 275–290.
[13] S. Rawat, N. Mitra, Compression twinning and structural phase transformation of single crystal titanium under uniaxial compressive strain conditions: comparison of inter-atomic potentials, Comput. Mater. Sci. 126 (2017) 228–237.
[14] H. Zong, T. Lookman, X. Ding, C. Nisoli, D. Brown, S.R. Niezgoda, S. Jun, The kinetics of the ω to α phase transformation in zr, ti: analysis of data from shock-recovered samples and atomistic simulations, Acta Mater. 77 (2014) 191–199.
[15] D. Brown, J. Almer, L. Balogh, E. Cerreta, B. Clausen, J. Escobedo-Diaz, T. Sisneros, P. Mosbrucker, E. Tulk, S. Vogel, Stability of the two-phase $\alpha\omega$ microstructure of shocked zirconium, Acta Mater. 67 (2014) 383–394.
[16] H. Zong, X. Ding, T. Lookman, J. Li, J. Sun, E.K. Cerreta, J. Escobedo, F.L. Addessio, C.A. Bronkhorst, Collective nature of plasticity in mediating phase transformation under shock compression, Phys. Rev. B 89 (22) (2014) 220101 .
[17] S. Rawat, S.P. Joshi, Effect of multiaxial loading on evolution of twinning in magnesium single crystals, Mater. Sci. Eng.: A 659 (2016) 256–269.
[18] S. Rawat, N. Mitra, Evolution of tension twinning in single crystal ti under compressive uniaxial strain conditions, Comput. Mater. Sci. 141 (2018) 302–312.
[19] S. Rawat, N. Mitra, Molecular dynamics investigation of c-axis deformation of single crystal ti under uniaxial stress conditions: evolution of compression twinning and dislocations, Comput. Mater. Sci. 141 (2018) 19–29.
[20] S. Rawat, P. Raole, Molecular dynamics investigation of void evolution dynamics in single crystal iron at extreme strain rates, Comput. Mater. Sci. 154 (2018) 393–404.
[21] S. Rawat, N. Mitra, Twinning assisted α to ω phase transformation in titanium single crystal, AIP Conference Proceedings, vol. 1832, AIP Publishing, 2017, p. 030018.
[22] Y.-M. Kim, B.-J. Lee, M. Baskes, Modified embedded-atom method interatomic potentials for ti and zr, Phys. Rev. B 74 (1) (2006) 014101 .
[23] R. Hennig, T. Lenosky, D. Trinkle, S. Rudin, J. Wilkins, Classical potential describes martensitic phase transformations between the α, β, and ω titanium phases, Phys. Rev. B 78 (5) (2008) 054121 .
[24] C. Tom, P. Maudlin, R. Lebensohn, G. Kaschner, Mechanical response of zirconium-i. Derivation of a polycrystal constitutive law and finite element analysis, Acta Mater. 49 (2001) 3085–3096.
[25] A. Salem, S. Kalidindi, S. Semiatin, Strain hardening due to deformation twinning in α-titanium: constitutive relations and crystal-plasticity modeling, Acta Mater. 53 (12) (2005) 3495–3502.
[26] A.A. Salem, S.R. Kalidindi, R.D. Doherty, Strain hardening of titanium: role of deformation twinning, Acta Mater. 51 (14) (2003) 4225–4237.
[27] I. Beyerlein, C. Tom, A dislocation-based constitutive law for pure zr including temperature effects, Int. J. Plast. 24 (2008) 867–895.
[28] S. Plimpton, Fast parallel algorithms for short-range molecular dynamics, J. Comput. Phys. 117 (1) (1995) 1–19.
[29] M.J. Suggit, A. Higginbotham, J.A. Hawreliak, G. Mogni, G. Kimminau, P. Dunne, A.J. Comley, N. Park, B.A. Remington, J.S. Wark, Nanosecond white-light laue diffraction measurements of dislocation microstructure in shock-compressed single-crystal copper, Nat. Commun. 3 (2012) 1224.
[30] A. Stukowski, V.V. Bulatov, A. Arsenlis, Automated identification and indexing of dislocations in crystal interfaces, Modell. Simul. Mater. Sci. Eng. 20 (8) (2012) 085007 .
[31] C. Barrett, M. Tschopp, H. El Kadiri, Automated analysis of twins in hexagonal close-packed metals using molecular dynamics, Scr. Mater. 66 (9) (2012) 666–669.
[32] A. Stukowski, Visualization and analysis of atomistic simulation data with ovito–the open visualization tool, Modell. Simul. Mater. Sci. Eng. 18 (1) (2009) 015012 .
[33] B.-Y. Liu, J. Wang, B. Li, L. Lu, X.-Y. Zhang, Z.-W. Shan, J. Li, C.-L. Jia, J. Sun, E. Ma, Twinning-like lattice reorientation without a crystallographic twinning plane, Nat. Commun. 5.
[34] S.J. Lainé, K.M. Knowles, {11 − 24} deformation twinning in commercial purity titanium at room temperature, Philos. Mag. 95 (20) (2015) 2153–2166.
[35] L. Capolungo, I. Beyerlein, Nucleation and stability of twins in hcp metals, Phys. Rev. B 78 (2) (2008) 024117 .
[36] J. Wang, J. Hirth, C. Tomé, (1 012) twinning nucleation mechanisms in hexagonal-close-packed crystals, Acta Mater. 57 (18) (2009) 5521–5530.
[37] M. Ghazisaeidi, W. Curtin, Analysis of dissociation of $< c >$ and $< c + a >$ dislocations to nucleate twins in mg, Modell. Simul. Mater. Sci. Eng. 21 (5) (2013) 055007 .
[38] L. Bao, C. Schuman, J.-S. Lecomte, M.-J. Philippe, X. Zhao, C. Esling, A study of twin variant selection and twin growth in titanium, Adv. Eng. Mater. 13 (10) (2011) 928–932.
[39] B.D. Cullity, J.W. Weymouth, Elements of x-ray diffraction, Am. J. Phys. 25 (6) (1957) 394–395.
[40] F. Qingsong, B. Wenji, Y. Jingsu, R. He, S. Nicheng, L. Guowu, X. Ming, M. Zhesheng, Titanium, ti, a new mineral species from luobusha, tibet, china, Acta Geol. Sin. (English Edition) 87 (5) (2013) 1275–1280 URL:http://rruff.geo.arizona.edu/AMS/minerals/Titanium.
[41] G. Gu, Y.K. Vohra, K.E. Brister, Phase transformation in titanium induced by laser heating at high pressure, Scr. Metall. Mater. 31 (2) (1994) 167–171.
[42] M. Yoo, S. Agnew, J. Morris, K. Ho, Non-basal slip systems in hcp metals and alloys: source mechanisms, Mater. Sci. Eng.: A 319 (2001) 87–92.
[43] E. Clouet, D. Caillard, N. Chaari, F. Onimus, D. Rodney, Dislocation locking versus easy glide in titanium and zirconium, Nat. Mater. 14 (2015) 931.
[44] L. Nervo, A. King, A. Fitzner, W. Ludwig, M. Preuss, A study of deformation twinning in a titanium alloy by x-ray diffraction contrast tomography, Acta Mater. 105 (2016) 417–428.
[45] A. Akhtar, Basal slip and twinning in α-titanium single crystals, Metall. Trans. A 6 (5) (1975) 1105–1113.
[46] J. Gong, A.J. Wilkinson, A microcantilever investigation of size effect, solid-solution strengthening and second-phase strengthening for $< a >$ prism slip in alpha-ti, Acta Mater. 59 (15) (2011) 5970–5981.
[47] P. Partridge, The crystallography and deformation modes of hexagonal close-packed metals, Metall. Rev. 12 (1) (1967) 169–194.
[48] J. Gubicza, Defect Structure in Nanomaterials, Elsevier, 2012.